GEOPHYSICS, VOL. 74, NO. 5 (SEPTEMBER-OCTOBER 2009); P. B183–B195, 11 FIGS., 2 TABLES.
10.1190/1.3205028

Case History

The 1998 Valhall microseismic data set: An integrated study of relocated sources, seismic multiplets, and S-wave splitting

K. De Meersman[1], J.-M. Kendall[2], and M. van der Baan[3]

ABSTRACT

We relocate 303 microseismic events recorded in 1998 by sensors in a single borehole in the North Sea Valhall oil field. A semi-automated array analysis method repicks the P- and S-wave arrival times and P-wave polarizations, which are needed to locate these events. The relocated sources are confined predominantly to a 50-m-thick zone just above the reservoir, and location uncertainties are half those of previous efforts. Multiplet analysis identifies 40 multiplet groups, which include 208 of the 303 events. The largest group contains 24 events, and five groups contain 10 or more events. Within each multiplet group, we further improve arrival-time picking through crosscorrelation, which enhances the relative accuracy of the relocated events and reveals that more than 99% of the seismic activity lies spatially in three distinct clusters. The spatial distribution of events and waveform similarities reveal two faultlike structures that match well with north-northwest–south-southeast-trending fault planes interpreted from 3D surface seismic data. Most waveform differences between multiplet groups located on these faults can be attributed to S-wave phase content and polarity or P-to-S amplitude ratio. The range in P-to-S amplitude ratios observed on the faults is explained best in terms of varying source mechanisms. We also find a correlation between multiplet groups and temporal variations in seismic anisotropy, as revealed by S-wave splitting analysis. We explain these findings in the context of a cyclic recharge and dissipation of cap-rock stresses in response to production-driven compaction of the underlying oil reservoir. The cyclic nature of this mechanism drives the short-term variations in seismic anisotropy and the reactivation of microseismic source mechanisms over time.

INTRODUCTION

The extraction of hydrocarbons changes the pressure within a reservoir and the surrounding rock formations. The resulting stress perturbations often reactivate faults and open or close fracture sets. Earthquakes or acoustic emissions that are generated in this way often are referred to as microearthquakes or microseismic events (Jupe et al., 2000). Because of the low magnitude of most microseismic events, passive seismic monitoring of reservoirs is usually done using well-based seismic arrays rather than surface arrays. This ensures the detection of more events as well as better data quality.

An important piece of information that can be obtained from the recorded data is the microseismic source locations. Microseismic events often occur in great numbers, and their source locations can form clusters that, resolution permitting, reveal fractures and faults. This information allows one to map active faults and is also useful for reservoir modeling because it can indicate directions of increased permeability and/or porosity (Maxwell et al., 1998; Audigane et al., 2002; Phillips et al., 2002; Shapiro et al., 2002). Microseismic source locations point to zones of mechanical instability — helpful information in planning and designing new wells (Kristiansen et al., 2000). Time-dependent variations and trends in the clustering of microseismic sources also have been used to monitor the growth and to determine the orientation of injection-induced fractures (Bell and Kaaijevanger, 2000; Maxwell and Urbancic, 2002).

Besides source locations, microseismic data also can be used to compute focal mechanisms and to obtain information on the local stress field (Nolen-Hoeksema and Ruff, 2001; House and Flores,

Manuscript received by the Editor 11 August 2008; revised manuscript received 10 March 2009; published online 18 September 2009.
[1]Formerly University of Leeds, School of Earth and Environment, Leeds, U. K.; presently CGGVeritas, Calgary, Alberta, Canada. E-mail: kristof.demeersman@cggveritas.com.
[2]Formerly University of Leeds, School of Earth and Environment, Leeds, U. K.; presently University of Bristol, Department of Earth Sciences, Bristol, U.K. E-mail: gljmk@bristol.ac.uk.
[3]Formerly University of Leeds, School of Earth and Environment, Leeds, U. K.; presently University of Alberta, Department of Physics, Edmonton, Alberta, Canada. E-mail: mirko.vanderbaan@ualberta.ca.

2002; Zoback and Zinke, 2002; Rutledge et al., 2004). Finally, S-wave splitting studies on microseismic data have linked spatial and temporal variations in seismic anisotropy to changes in the local stress field and fracture properties (Teanby et al., 2004; Al-Anboori et al., 2005).

Pavlis (1992) argues that the precision of earthquake locations is mainly a function of the source-receiver configuration, the accuracy of the velocity model, and arrival-time picking. Although some techniques based on waveform inversion do not require picked arrival times to compute source locations (Kao and Shan, 2004; Gajewski and Tessmer, 2005), most methods determine source locations by minimizing the difference between observed and predicted arrival times of various phases at several receivers. Location accuracy can improve significantly with relative relocation techniques (Got, 1994; Waldhauser and Elsworth, 2000; Moriya et al., 2003). Such techniques usually rely on the presence of seismic multiplets within the data set. Seismic multiplets are earthquakes generated on a single fault by the same mechanism (Geller and Mueller, 1980). Consequently, their waveforms are extremely similar; once identified, they can be used to obtain highly accurate relative arrival times by cross-correlation (Schaff et al., 2004). Multiplets also are useful for investigating time-dependent variations in the velocity field and for studying seismic attenuation (Poupinet et al., 1984; Frémont and Poupinet, 1987).

In this work, we relocate and investigate the microseismic sources recorded as part of an experiment in the Valhall oil field (Dyer and Jones, 1998; Dyer et al., 1999), central North Sea Graben (Figure 1). The reservoir consists of the Tor and Hod Formations, which are overpressured, undersaturated Late Cretaceous chalks. The siltstone overburden has limestone stringers (Leonard and Munns, 1987). Production-induced reservoir compaction and subsidence (over 4 m at the seabed) are believed to be the main reason for microseismic activity (Dyer et al., 1999).

The Valhall experiment lasted 57 days in June and July 1998. It used a six-station, three-component (3-C) vertical geophone array placed in a vertical well near the crest of the field (Figure 1). We refer to the receivers as stations 1–6, with numbers increasing from top to bottom. The 3-C receivers were installed at 20-m intervals and between depths of 2100 and 2200 m below mean sea level — approximately 250 m above the top of the reservoir. A total of 572 microseismic events were recorded, of which 324 were located by Dyer et al. (1999). For reasons of data quality, we consider only 303 events.

Most events are located in a 50-m-thick zone above the reservoir. The microseismic source locations also form two diffuse yet distinct clusters. Jupe et al. (2000) argue that the elongate direction of these clusters is roughly northwest–southeast and southwest–northeast, agreeing with the general fault pattern for Valhall. Maxwell (1999) argues that the velocity model used by Dyer and Jones (1998) is too slow and then relocates the Valhall microseismic events using several alternative velocity models. Maxwell (1999) concludes that reasonable changes in the velocity model result in sources that locate up to 55 m deeper, or within the reservoir, whereas changes in location misfit values are minimal. Nonetheless, the separation of source locations into two distinct clusters is a robust feature.

In this work, we use the same velocity model and location software as do Dyer and Jones (1998) and Dyer et al. (1999). This allows us to isolate the effect of improved arrival-time and polarization picking. Also, this original velocity model places the events in the reservoir overburden, a region likely to produce microearthquake activity because of the high incidence of well-casing deformations and well losses as a result of faulting (Kristiansen et al., 2000). We improve the accuracy of the source locations by using more precise methods for obtaining P- and S-wave arrival times and P-wave polarizations, or P-wave particle motion directions as observed on hodograms.

For each event, we apply an iterative crosscorrelation method to reduce the relative picking error between the respective arrivals on the different receivers. The subsequent use of array stacks, or beams, with increased signal-to-noise ratio (S/N) lets us obtain a more accurate definition of the absolute arrival time for both phases. This is especially so for several events for which the S-wave first motion is unclear and difficult to pick. The P-wave polarizations are repicked using an automated array-based singular-value decomposition (SVD) method as per De Meersman et al. (2005).

The data are then subjected to multiplet analysis to detect and group events with similar waveforms and P-to-S traveltimes. Once a multiplet group is identified, we can improve the relative arrival-time picking between its members. For this, we use the same iterative crosscorrelation approach initially used to improve the relative alignment between arrivals on different receivers. This leads to source locations with better relative accuracy within each multiplet group. The combination of more accurate and better-resolved source locations with the information provided by the different multiplet groups allows us to reinterpret the microseismicity with greater reliability.

Finally, we attempt a combined interpretation of our work with the S-wave splitting results from Teanby et al. (2004).

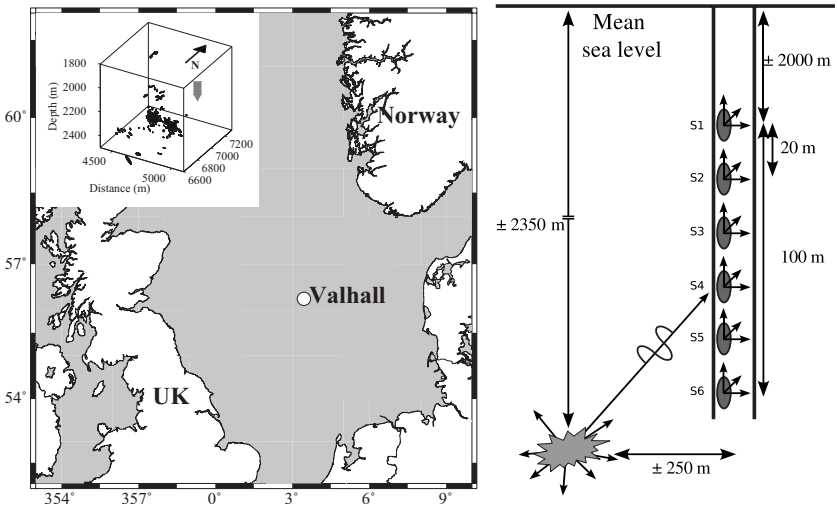

Figure 1. (Left) Valhall location map with 3D inset, reporting the locations of the microearthquake sources recorded during a 1998 experiment (after Dyer et al., 1999). (Right) General geometry overview of the 1998 experiment. The geophone stations were deployed at 20-m intervals between 2000 and 2100 m, and are numbered 1–6 with increasing depth.

ABSOLUTE RELOCATION

Earthquakes typically are located using a velocity model and P- and S-wave arrival times at different receivers. The Valhall experiment uses a single, vertical receiver array. Therefore, source locations can be determined only if the P-wave polarizations are included to constrain the source back azimuth. We relocate the microseismic events with the software used by Dyer and Jones (1998). Sources are located on a grid by searching for the position where the difference between observed and ray-traced P- and S-wave arrival times and P-wave polarizations is minimal. In comparison to the original locations of Dyer and Jones (1998), we recompute the source locations of the microseismic events using (1) repicked, more accurate P- and S-wave arrival times and (2) new P-wave polarization estimates.

The size/aperture of the receiver array with respect to the nominal source-receiver distance is relatively small for this experiment. The waveforms, amplitudes, and propagation vectors of the incoming waves therefore vary only slightly between the receiver stations. Although this may be restrictive in many ways, one major advantage is that it allows us to use crosscorrelations between stations in combination with array stacking to improve the accuracy of arrival times and P-wave polarizations.

P- and S-wave arrival times

The P- and S-wave arrival times are repicked independently using an iterative crosscorrelation procedure, similar to that proposed by Ronen and Claerbout (1985) and Rowe et al. (2002). Figure 2 gives a graphical explanation of our method for a P-wave example. The left column shows the P-wave for a representative event as it is recorded at the six receiver stations. The vertical markers indicate the manually picked arrival times as in Dyer and Jones (1998). For stations without picked arrival times, we use an interpolated estimate or discard it if the available data are deemed to be of too poor quality. The middle column shows the aligned P-wave data; the resulting 3-C array stack is shown at the bottom. The alignment, or moveout correction, is based on the initial P-wave picks. Before stacking, the data from each station are rescaled to equalize the pre-event noise level.

From the 3-C stack trace, we then take a 100-ms-long window, centered on the picked arrival, to use as a pilot trace and correlate it with the data from each individual station. The maxima on the resulting 3-C crosscorrelation functions indicate the arrival-time corrections needed to optimally realign the data at each station with the pilot trace. The right column in Figure 2 shows the data after the arrival-time corrections have been applied. A new array stack and pilot are calculated, and the crosscorrelations are repeated. It usually takes less than three iterations for the arrival-time corrections to converge to zero.

This process optimizes the relative picking accuracy between stations. The absolute arrival times are improved by repicking them manually on the final 3-C stacked trace. In theory, this stack should have an S/N that is approximately $\sqrt{6}$ times higher than those at individual stations, thereby permitting a more accurate definition of the absolute arrival time.

P-wave polarizations

The P-wave polarization estimates used for our event relocation are taken from a study by De Meersman et al. (2005). In the 2005 study, an automated method for polarization analysis on seismic arrays is used. It simultaneously estimates the polarizations for all stations within an array using a noise-weighted SVD of the complex analytic signals from all 3-C receivers. The combination of a weighting scheme based on pre-P-wave noise and the simultaneous analysis of all receivers within the array enables this method to provide more accurate polarization estimates in the presence of polarized background noise.

In comparison, Dyer and Jones (1998) determine polarizations at each station by applying an SVD to a hand-picked data window. De Meersman et al. (2005) compare both sets of estimates and find that polarized background noise in data from station 5 likely affect some polarization estimates in the original analysis. The bias in Dyer and Jones (1998) is less than 5° and does not affect our estimates. Our relocation is calculated using 1463 polarization estimates, spread over six stations and 303 events, with a typical 95% confidence angle of 3°.

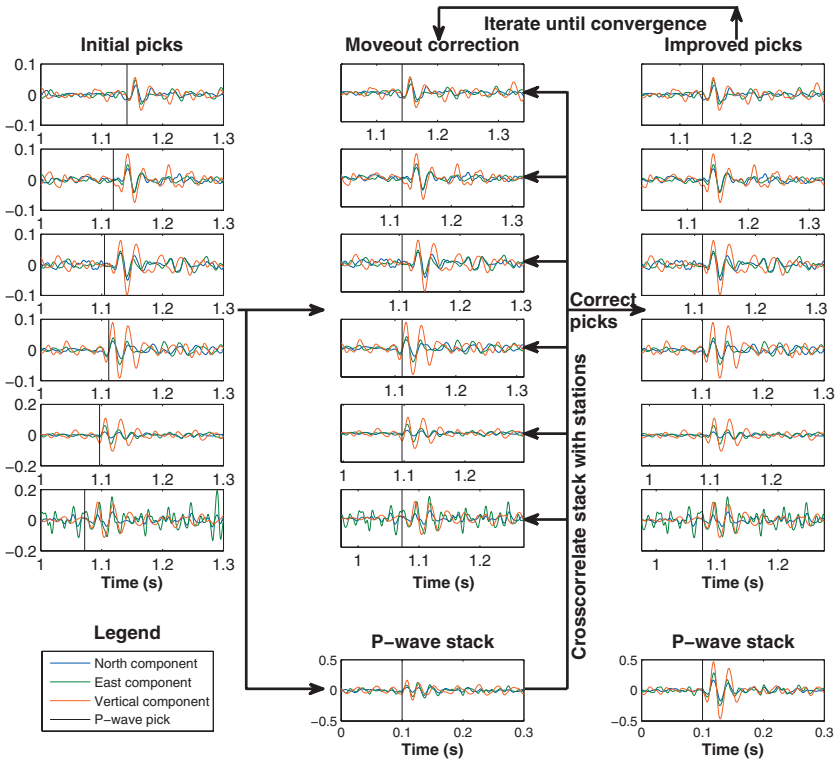

Figure 2. Improved P- and S-wave arrival-time picking by crosscorrelation, demonstrated for a P-wave. Initial picks from Dyer and Jones (1998) are used to correct for moveout along the array and to calculate a preliminary 3-C stack. This stack is crosscorrelated with the moveout-corrected signals from each station. In turn, this provides arrival-time corrections at each station. These are applied to the initial picks to improve stack quality. The process is repeated until the arrival-time corrections converge to zero.

A subsequent quality-control (QC) step of the polarization estimates reveals that they possibly were affected by a more severe bias related to acquisition rather than noise or the measuring technique. The receiver tools in this survey were not fitted with an internal positioning and orienting system. This makes it difficult to monitor possible changes in the orientation and position of the 3-C geophones while recording. The direction of the horizontal geophone components was determined in the second week of acquisition, using signals from an air-gun source fired in a circular pattern around the borehole. The vertical geophones align with the well, which is vertical (Dyer and Jones, 1998).

The vertical receiver array was deployed in an approximately 1D local-velocity structure, so we can expect that all receiver stations should provide the same P-wave back-azimuth estimates for any given microseismic event. In Figure 3a, we show the P-wave back-azimuth residuals per station as a function of time. A histogram of the residuals for each station also is given. The residuals are defined as the angles between the measured back azimuth for an event and station and a reference back azimuth for that event. We take the average back azimuths of stations 4 and 5 as reference because they are the most similar to one another. Residuals from geophones 4–6 have a symmetric, Gaussian distribution around zero, with standard deviations of 2.5°, 2.5°, and 4.8°, respectively. In contrast, residuals in stations 1–3 decrease exponentially over the first 20–30 days of the experiment. The change is quite dramatic because residuals in these respective stations decrease by approximately 40°, 30°, and 15°. They also are accompanied by larger standard deviations of 12.7°, 10.5°, and 6.9°.

The observed behavior, especially the magnitude and time scale, is difficult to explain in terms of changes in local geology. The most likely causes are time-dependent changes in geophone coupling and/or a rotation of the geophone tools. A gradually changing clamping

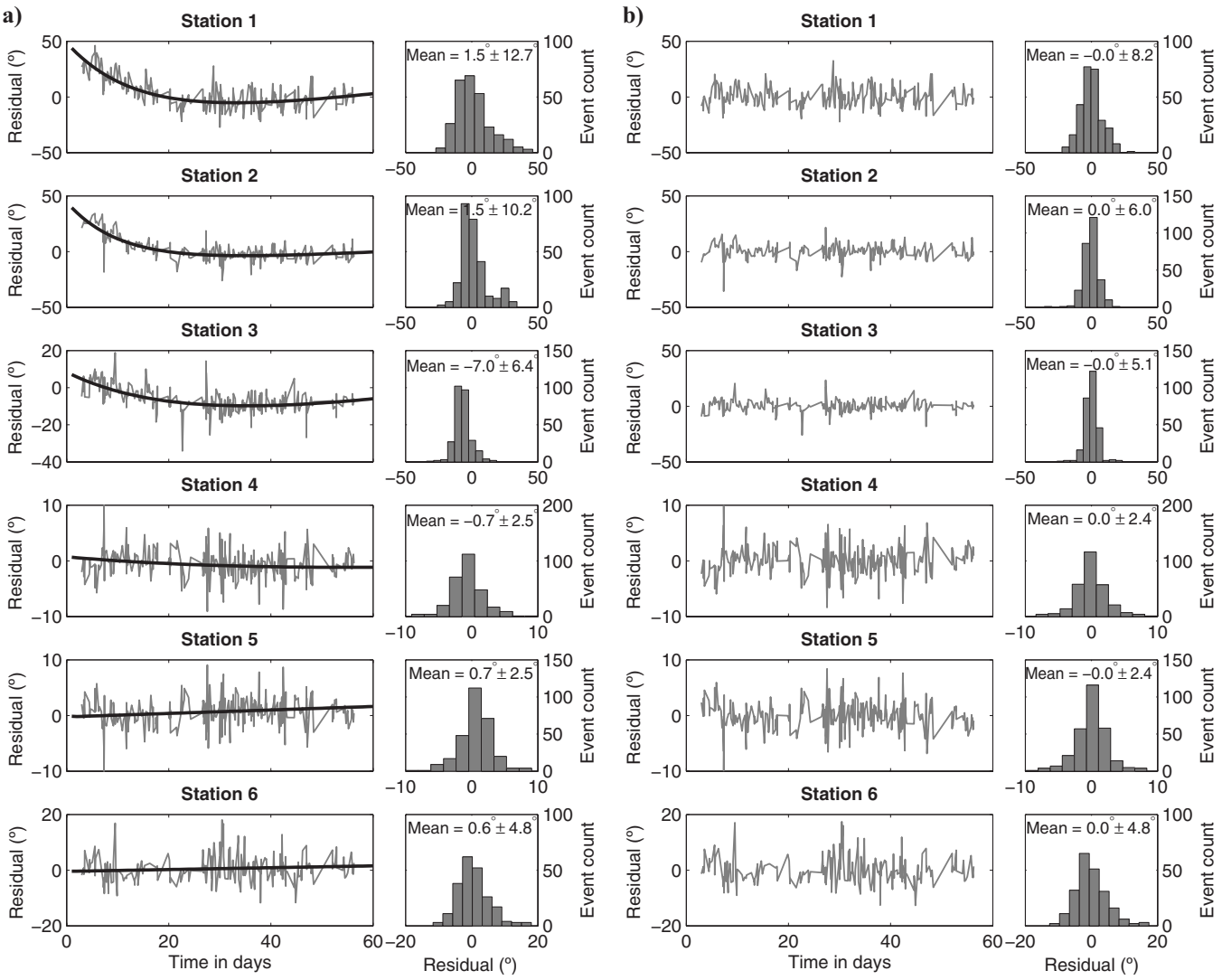

Figure 3. P-wave back-azimuth residuals as a function of time for each station. For each event, the residuals are given with respect to average P-wave back azimuth from stations 4 and 5. These stations were chosen as a reference because their azimuth values show the least variability with time. Histograms of the azimuth residuals are also shown. (a) Values based on repicked P-wave polarizations. Over the first 30 days, the P-wave back azimuths in stations 1–3 are up to 30° larger than those in the reference stations. This most likely is caused by geophones rotating inside the well. We estimate the relative movement by fitting a function $y = ae^{bt} + ct + d$ to the residuals at each station and use this to apply a P-wave polarization azimuth correction. (b) P-wave back-azimuth residuals after correction for geophone rotations.

pressure can affect the coupling in each station differently and generate the anomaly. Furthermore, the clamping pressure was increased gradually at the start of the experiment (R. Jones, personal communication, 2001). However, an impulse test was conducted each day to check tool coupling. These tests found no significant coupling changes throughout the monitoring (Dyer and Jones, 1998). Another argument against coupling effects is that unreasonably large coupling differentials would be needed. We conclude that geophone movement during the first 30 days of the experiment is the most probable source for the observed bias.

For each station, we compute a time-dependent azimuth correction to remove the rotating geophone bias by least-squares fitting the curve $y = ae^{bt} + ct + d$ to the anomalies in Figure 3a. The time in days is represented by t. The P-wave back-azimuth residuals for each station after correction are given in Figure 3b. Now the residuals are approximately randomly distributed around zero, with standard deviations of 8.2°, 6.0°, 5.1°, 2.4°, 2.4°, and 4.8° for geophone stations 1-6.

Relocated sources

In Figure 4, we compare our source locations with those reported by Dyer et al. (1999). Our relocated sources in Figure 4b are computed using the same location software and velocity model as for the original locations in Figure 4a. The differences between the old and new locations depend entirely upon changes in the picked arrival times and the measured polarizations. The source locations in Figure 4a and b are represented by their 68% confidence ellipsoid. On average, these confidence ellipsoids are 50% smaller than those for the original locations. This translates to a twofold increase in location accuracy. The two previously identified source clusters also are better separated spatially and have become smaller. For cluster 1, which is nearest to the array, this size reduction is approximately 50%. The new locations are also on average 15 m closer to the center of the receiver array.

An important observation with respect to geophone corrections is a negligible average azimuthal shift of approximately 3° in our locations. This supports the idea that the correction for geophone rotations is appropriate and accurate. The new locations reveal the existence of a previously undetected third cluster, approximately 500 m to the northwest of the receiver array. Two additional smaller clusters are to the southwest and south-southwest. Locations within these clusters are significantly more uncertain than those in clusters 1 and 2.

From these observations, we conclude that at least five seismically active fault zones are needed to explain the observations — not two, as interpreted by Dyer et al. (1999), Kristiansen et al. (2000), and Zoback and Zinke (2002).

MULTIPLET ANALYSIS, RELOCATION, AND INTERPRETATION

Multiplets consist of at least two earthquakes with the same source mechanism and source location. The members of a multiplet typically have very similar waveforms and can be identified by means of their high crosscorrelation coefficients (Geller and Mueller, 1980; Poupinet et al., 1984). One advantage of finding multiplets in a data set is that it allows for a more precise relative relocation of the sources within each group and sometimes even between different multiplet groups (Waldhauser and Elsworth, 2000). We can achieve this precision by using more accurate relatively picked P- and S-wave arrival times. These can be obtained by crosscorrelating the picked phases from events within each multiplet (Hemmann et al., 2003).

Multiplet analysis

Our multiplet analysis uses the array-averaged time-domain crosscorrelation functions for each pair of microseismic events. At each station, the crosscorrelation function between two events is cal-

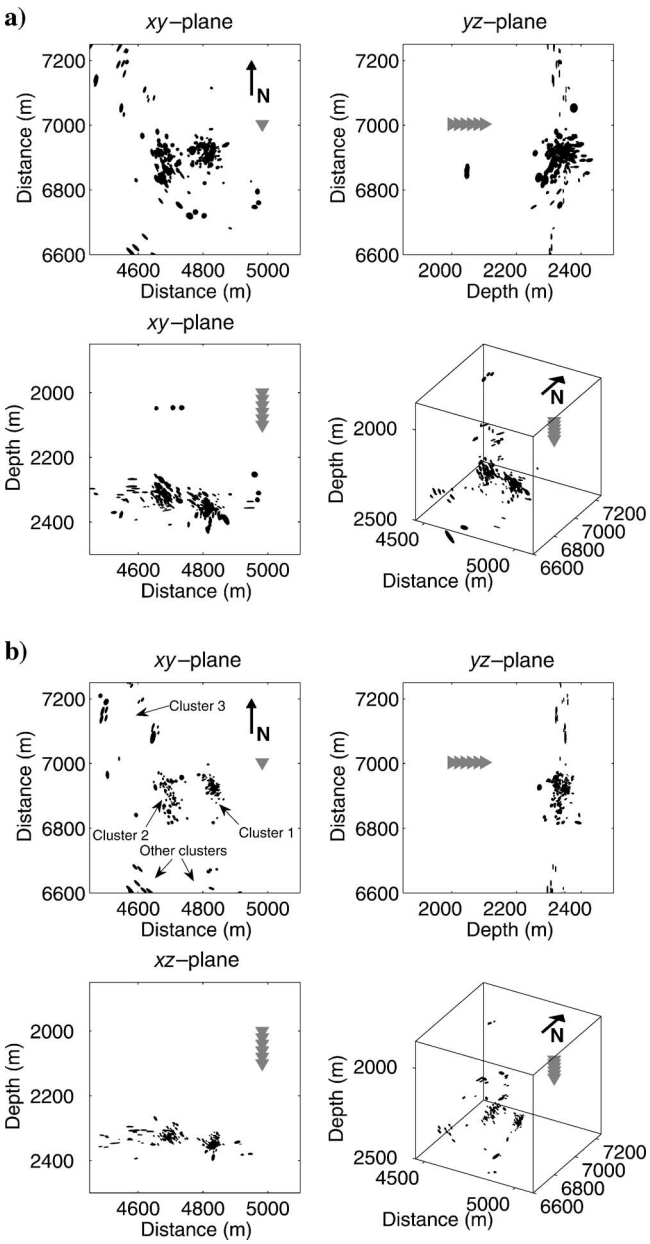

Figure 4. Source locations for 303 events with error ellipsoids. (a) Locations obtained from arrival times and P-wave polarizations by Dyer and Jones (1998). (b) Relocated events after using crosscorrelation repicking of P- and S-wave arrival times and P-wave polarizations. These polarizations are corrected for the bias from poorly clamped and rotating geophones. The geophone locations are indicated by gray triangles. Five source clusters can be interpreted.

culated using 500 ms of data and starting 20 ms before the respective P-wave arrival. This data window also includes the S-wave arrival with part of its coda. For each microseismic event pair, we then normalize the correlation functions from the different receivers and sum them to obtain the array-averaged crosscorrelation functions. For reasons of data quality, we limit our analysis to 303 events and reject any data recorded on the lowermost sixth receiver. Finally, we prefilter the data using a 60-Hz high-cut filter.

For each event pair, we can store the maximum correlation coefficient in a symmetric matrix (Got, 1994; Scarfi et al., 2003). The correlation matrix for Valhall (Figure 5a) contains 303×303 color-coded cells. The cell color varies from red for correlation coefficients of one to blue for coefficients of zero. The events are ordered chronologically from left to right and top to bottom. The red diagonal consists of the autocorrelation coefficients. Chronologically ordered correlation matrices such as the one in Figure 5a often appear disorganized. This is because events from the same multiplet generally occur at random times during acquisition.

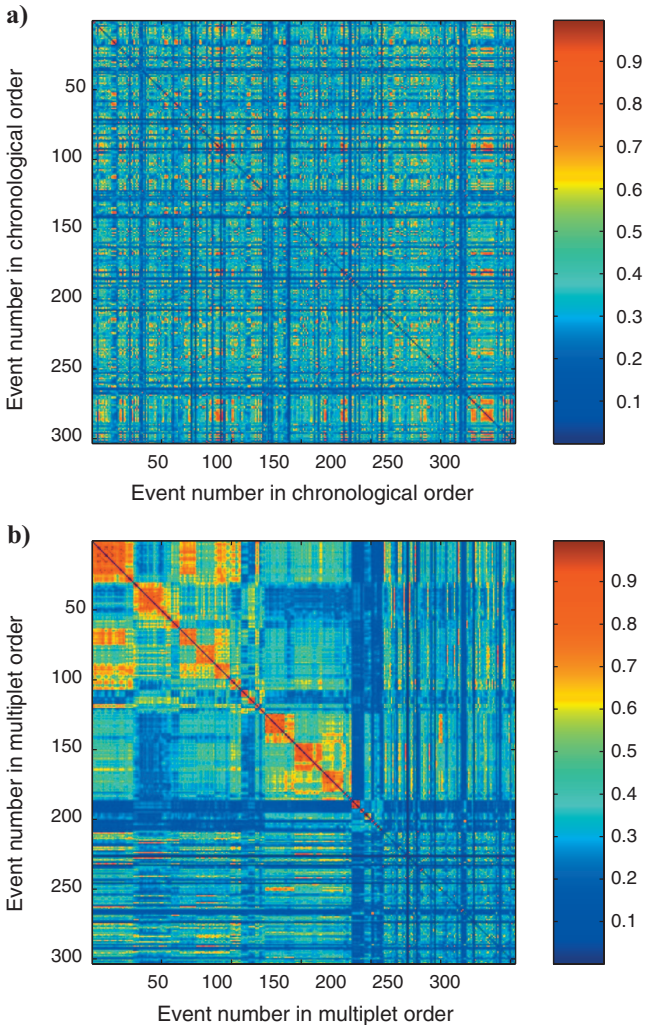

Figure 5. Matrix of crosscorrelation coefficients between the 303 relocated Valhall events. Each cell gives the maximum correlation coefficient between any two events. A cell is blue for a correlation coefficient of zero and red for a coefficient of one. (a) Crosscorrelation coefficients for events in chronological order. (b) Crosscorrelation coefficients for events sorted by source cluster and into multiplet groups. The first 124 events belong to 19 multiplets in source cluster 1, the next 62 belong to 13 multiplets in source cluster 2, and the 22 remaining events belong to 8 multiplets in source cluster 3. The source clusters are annotated in Figure 4.

We define our multiplets as exclusive groups of events for which the average crosscorrelation coefficients exceed a predefined threshold. The correlation threshold must be chosen to balance two counteracting objectives, each of which depends strongly on the noise level. The first objective is the ability to form multiplet groups by choosing a threshold that is sufficiently low. Typically, data with high noise levels require low correlation thresholds. The second objective is the ability to differentiate between multiplet groups by choosing a high-enough threshold. For our analysis, we use a correlation threshold of 80%. We identify 40 multiplet groups that account for 208, or approximately 66%, of all recorded events. The largest group has 24 members; another five groups have 10 members or more.

The chronological correlation matrix in Figure 5a can be reordered to group events from each multiplet. The resulting multiplet-sorted correlation matrix for Valhall is shown in Figure 5b. The multiplets now appear as highly correlated red squares along the diagonal. We also group multiplets located in approximately the same position and moderately correlated by more than 60%. We define these as multiplet supergroups. Most multiplets are part of the two largest source clusters (see Figure 4a). A summary of the organization of multiplet groups into multiplet supergroups and clusters is provided in Table 1.

Similar multiplet analysis has been done on these data by Arrowsmith and Eisner (2005). They define a multiplet as a group of events where each event is well correlated with at least one other event in the group. Each multiplet is then divided into subgroups of highly similar events. This is contrary to our approach, where we start with highly correlated groups of events and then consider spatial clusters of these groups.

Multiplet relocation

Multiplet analysis often precedes a relative source relocation. In many cases, this is done by inverting highly accurate relative arrival times between all events and one or more reference events for small location perturbations (Got, 1994; Waldhauser and Elsworth, 2000; Wolfe, 2002; Lin and Shearer, 2005). These relative arrival times can be obtained to subsample precision by crosscorrelating sinc-interpolated P- and S-wave arrivals from different events. Unfortunately for Valhall, the relative relocation methods mentioned are of little use because they require a 2D receiver array or better.

The relative relocation method proposed by Moriya et al. (1994) includes estimates of P-wave polarizations to compensate for inadequate receiver geometries. Although this method is intended for single-station relocation and assumes straight rays, it can be generalized for more complex velocity fields and multiple recording stations. For the Valhall data, the accuracy needed for the P-wave polarization differences between events is approximately 1° and cannot be achieved. The only alternative is to compute new absolute source locations for the multiplet events using high-precision relatively repicked arrival times.

To repick P- and S-waves, we modify the approach used initially to pick a single arrival at different receivers in the vertical array (Figure 2). The main difference is that arrival times within each multiplet group are now fine tuned by correlating P-wave (or S-wave) windows from all receivers and multiplet members with a single 3-C pi-

lot trace. This multiplet pilot trace is found by stacking the data over all receivers and multiplet members. Because P-to-S-wave arrival-time differences within multiplet groups are small (typically 2–3 ms) compared to the sampling rate of the data (1 ms), we Fourier interpolate the data to a sampling rate of 0.2 ms. Relative arrival times can now be estimated accurately to a subsample precision of 0.2 ms between members and stations of the same multiplet group. We also manually QC the absolute arrival times for all events within a multiplet group on the final pilot trace for each multiplet group and phase.

Figure 6 shows the locations for multiplet events belonging to the three main source clusters. For reference, these clusters are identified on Figure 4b. The source locations in Figure 6a are a subset of those in Figure 4b. Using the new subsample precision and relatively repicked multiplet arrival times, we relocate these events with the results shown in Figure 6b. The colors with which these locations are plotted indicate the multiplet supergroup to which the events belong. A summary of multiplet supergroups and their plot color is given in Table 1.

The use of more accurate P- and S-wave arrival times to compute the locations in Figure 6b further reduces the size and scatter within the two largest source clusters when compared to the locations in Figure 6a. This is not so for the third source cluster, located farther to the northwest. Note that the locations in Figure 6a already represent a significant improvement upon the original locations in Figure 4a and by Dyer et al. (1999).

Close inspection of the two main clusters on the *xy*-plane in Figure 6b shows distinct subclusters of events with the same color. This is especially so for the largest cluster, cluster 2. The subclusters are formed by events that belong to the same multiplet supergroup and are relatively small, with typical radii in the 10–30-m range. The position of events in the *xy*-plane is constrained mainly by the P-wave polarization, which is unaffected by multiplet analysis. In other words, if unrelated events had been assigned to the same multiplet group or supergroup, then we would not observe the formation of subclusters. Hence, the existence of these subclusters increases the reliability of our multiplet analysis and any conclusions based thereupon.

As a final comment, we point out that no multiplet events have been relocated inside the reservoir. This is contrary to studies by Dyer et al. (1999) and Maxwell (1999), who report a few events with locations inside the reservoir.

Interpretation of results

Using 3-C P- and S-wave multiplet stacks (Figure 7), we can gain a better understanding of the relationships and interactions between different multiplet groups within each cluster. These 3-C stacks are obtained by summing the data from all receivers and events belonging to the same multiplet group. The range in source back azimuths of the stacked data is typically less than 10°, and variations in P-to-S amplitude ratios are minimal. Therefore, the 3-C stacks can be used to make meaningful qualitative comparisons between the average P-to-S amplitude ratios from different multiplet groups. To facilitate this, we also normalize the data by applying an equal scaling to the P- and S-wave stacks from each multiplet as well as rotating the data into a P-wave ray-centered coordinate system. The normalization is

Table 1. Multiplet properties. Cluster 1 — nearest to geophone string. Cluster 2 — farther from the geophone string. Cluster 3 — newly identified and farthest from the geophones. All location clusters are to the east of the receiver tool.

Multiplet group	# events in group	Cluster	Super group	Plot color in Figure 6	Multiplet group	# events in group	Cluster	Super group	Plot color in Figure 6
1	24	1	A	Dark blue	21	2	2	F	Dark blue
2	6	1	A	Dark blue	22	2	2	F	Dark blue
3	4	1	B	Light blue	23	3	2	F	Dark blue
4	16	1	B	Light blue	24	13	2	G	Yellow-green
5	4	1	B	Light blue	25	4	2	G	Yellow-green
6	3	1	B	Light blue	26	3	2	G	Yellow-green
7	6	1	C	Light green	27	9	2	H	Red
8	12	1	C	Light green	28	4	2	H	Red
9	13	1	D	Red-orange	29	2	2	H	Red
10	9	1	D	Red-orange	30	2	2	—	Gray
11	2	1	D	Red-orange	31	2	2	—	Gray
12	4	1	E	Brown	32	2	2	—	Gray
13	2	1	E	Brown	33	6	3	—	Gray
14	2	1	E	Brown	34	3	3	—	Gray
15	5	1	—	Gray	35	3	3	—	Gray
16	5	1	—	Gray	36	2	3	—	Gray
17	3	1	—	Gray	37	2	4	—	Gray
18	2	1	—	Gray	38	2	5	—	Gray
19	2	1	—	Gray	39	2	3	—	Gray
20	14	2	F	Dark blue	40	2	3	—	Gray

such that within each multiplet group, the maximal amplitude of the most energetic phase is set to one. The rotation into ray-centered coordinates is illustrated in Figure 8.

Cluster 1

Cluster 1 is located nearest the receiver array and is composed of multiplet groups 1–19. Of these, we assign 14 groups to five supergroups of related multiplets (Table 1). On Figure 7, we observe strong similarities between the P-wave stacks from all multiplets in this cluster. The waveforms are nearly identical and thus are the apparent first motions. In sharp contrast to this, we observe large variations in P-to-S amplitude ratios between the five previously identified multiplet supergroups. For supergroup B (multiplets 4–6), the P-to-S amplitude ratio is significantly greater than one. This is contrary to multiplets from supergroup D (multiplets 12–14), where P-to-S amplitude ratios are significantly less than one. The remaining multiplet groups in this cluster have P-to-S amplitude ratios that are close to unity.

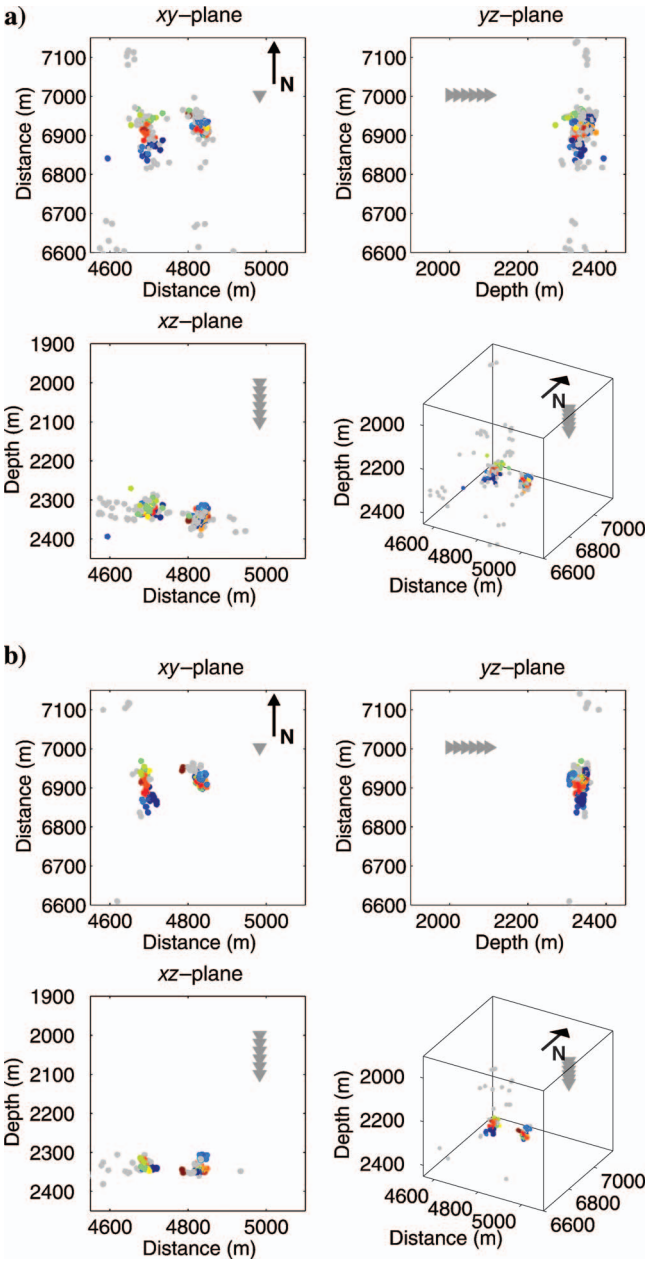

Figure 6. (a) Multiplet locations after crosscorrelation repicking and geophone rotation corrections. The locations are identical to those in Figure 4b, but only the 208 multiplet events are shown. The colors indicate the multiplet group as per Table 1. (b) Multiplet locations after crosscorrelation arrival-time repicking between the events in each multiplet group. The geophone locations are indicated by gray triangles.

Such large variations in P-to-S amplitude ratio are especially important given the limited range in source back azimuths for the events in this cluster. The back azimuth of most events lies within a narrow window of approximately 20° and typically 55°–76°. The range in inclinations is more restricted and varies between approximately 55° and 62°. Differences between multiplets that belong to the same supergroup are more subtle and arise mainly from slight variations in S-wave energy partition between the *x*- and *y*-components and/or S-wave polarity. A good example of the latter is supergroup C, which consists of groups 7 and 8. These multiplets are more or less colocated and have nearly identical P- and S-waves. They only differentiate by an S-wave polarity reversal on *x*- and *y*-components.

Based on these observations, we conclude that the microseismic activity in this cluster is very likely generated by a single fault (zone). The strongest argument in favor of this is the evident similarities between the P-waves from events in this cluster. The differences within multiplet supergroups are very subtle and probably relate to different asperities on which displacement takes place. However, it is impossible to ignore the strong variations in P-to-S amplitude ratios between multiplet supergroups. Given the small range in source back azimuths from where the amplitude ratios are measured, we find it highly unlikely that the data can be explained in terms of a single source mechanism or common focal sphere. The microseismic activity is most likely generated by a single fault zone in which a few different source mechanisms repeat over time.

Cluster 2

The multiplets in cluster 2 have back azimuths of approximately 60°–79° and inclinations of approximately 37°–45° (Figure 7, groups 20–32; Figure 6b). Three multiplet supergroups are within this cluster. Contrary to cluster 1, there is little variation in the P-to-S amplitude ratios, which are typically ≤ 0.5. There are also more dissimilarities between the P-waveforms from the different multiplet groups. This could be attributable partly to the generally low P-wave amplitudes and hence low S/N. There are even some suggestions of P-wave polarity reversals, e.g., within supergroup H between multiplets 27 and 28 (Figure 7). The S-wave stacks for this cluster are fairly similar. The differences between the multiplets are mainly the result of variations in phase content and energy partition between the *x*- and *y*-components. When we compare the S-waveforms from supergroups F (20–23) and H (27–29) with those of supergroup G (24–26), the S-waves appear to have reversed polarity.

Based on waveform similarities (mainly S-waves) and the tight range of P-to-S amplitude ratios, we find it likely that the sources in cluster 2 relate to the same fault plane and that they were generated by a similar focal mechanism. Furthermore, the typically small P-to-S amplitude ratios and the observations of some polarity reversals seem to indicate that the source back azimuths lie close to one of the nodal planes of the average focal sphere for this cluster.

Cluster 3

Cluster 3 contains six multiplet groups (34, 35, 36, 37, 39, 40), totaling 20 events. There are significantly more intermultiplet waveform differences between the groups in this cluster, which explains why no supergroups could be identified. The S-wave and some P-wave arrivals are also less clear and more affected by noise. The P-to-S amplitude ratios vary from just above one to less than 0.5. An in-depth interpretation of this cluster is not advisable at this stage, given the few events as well as the significant dissimilarities between its multiplets.

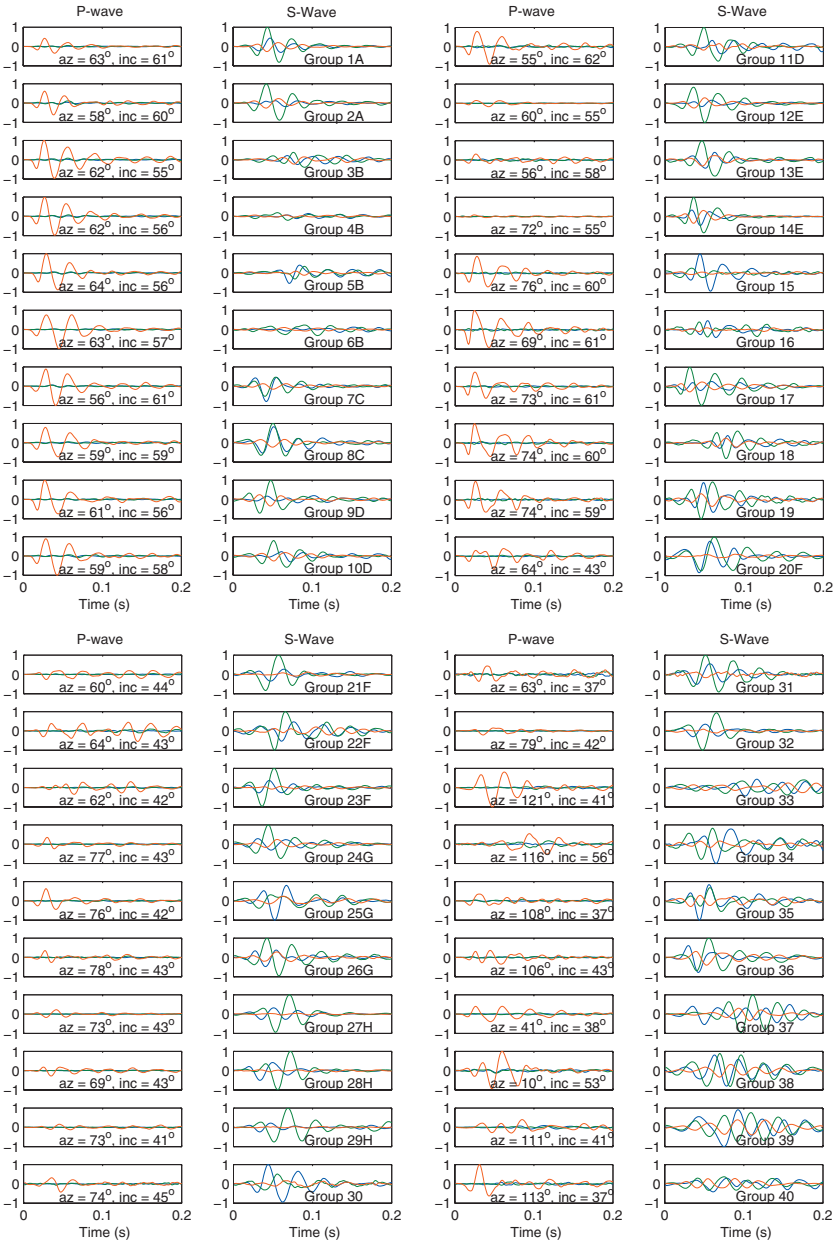

Figure 7. Multiplet P- and S-wave stacks for multiplet groups 1–40. Each 3-C stack is generated by summing data from all stations in the multiplet and rotating the data into a ray-centered coordinate system (see Figure 8). The P- and S-wave stacks of each multiplet are scaled equally so that the maximum amplitude of the most energetic phase is normalized. The range in source back azimuths of the stacked data within each multiplet is less than 10°. The stacks therefore accurately reflect the averaged P-to-S amplitude ratios for each multiplet. Multiplets 1–19 are located in cluster 1, 20–32 in cluster 2, multiplets 33–36 and 39–40 in cluster 3, and 37–38 in the remaining two clusters (see Table 1).

Inferred fault planes from locations in clusters 1 and 2

Our interpretation shows that the microseismic sources in clusters 1 and 2 are part of two separate faults or fault zones. Information on the position and orientation of the fault planes can be found by least-squares fitting a plane through the source locations from each cluster. The resulting fault planes and the locations of the sources used to calculate them are shown in Figure 9. UTM coordinates of the plane midpoints and their strike and dip directions are given in Table 2. Both faults strike approximately north-northwest–south-southeast and have opposite near-vertical dips.

We independently verify our inverted fault planes using external information in the form of a top-reservoir fault map obtained from interpreting 3D surface seismic data (O. I. Barkved, personal communication, 2005). Figure 10 shows a section of this fault map, overlain with the sources from clusters 1 and 2. The events from each cluster locate along two distinct, subparallel faults. Moreover, the strikes of the least-squares fitted fault planes agree remarkably well with the fault trends inferred from the structure map. Our results contradict the findings of studies using the same data and which suggest northeast–southwest-trending fault strikes (Dyer et al., 1999; Jupe et al., 2000; Kristiansen et al., 2000; Zoback and Zinke, 2002).

An interesting observation on Figure 10 is that the northern edge of cluster 1 is located on a T-junction between a major north-northwest–south-southeast-trending fault and another east-northeast–west-southwest-trending fault. The latter fault terminates at the first. Although speculative, it seems plausible that the events in this cluster are generated along the edges of two orthogonal fault planes. This could explain the range of P-to-S-amplitude ratios observed between multiplets in this cluster.

DISCUSSION

Teanby et al. (2004) analyze the Valhall microseismic events for S-wave splitting and find clear evidence for S-wave anisotropy that varies spatially and with time. The spatial variations in S-wave splitting are observed mostly between the two main source clusters. Temporal variations in S-wave splitting are observed mostly within the cluster nearest to the receiver array. Teanby et al. (2004) argue that the most probable causes for these changes are variations in stress and pore pressure, resulting from tidal loading and/or oil production.

In Figure 11, we compare the S-wave fast direction and percentage anisotropy as per Teanby et al. (2004) within multiplet supergroups C and D. Other multiplet groups could not be compared because of too few events for which we have splitting estimates. Between multiplets 7 and 8 from group C, we observe systematic differences in the percentage anisotropy (≈1.5% versus ≈0.5%) and the fast direction from north (≈120° versus ≈50°). For supergroup D with multiplets 9 and 10, we get similar values for the fast direction of ≈80° from north. The percentage anisotropy for multiplet 9 is ≈0.75%; for multiplet 10, it is ≈2%.

In general, variations in S-wave splitting between two events can be caused by (1) travel-path differences in a medium with spatially varying anisotropic properties and (2) time-variant changes in the anisotropic properties of a medium or (3) a combination of both. Events within both multiplet supergroups are located closely and are generated by similar source mechanisms. Therefore, path differences can be excluded as the main cause for the observed variations in S-wave splitting. The most likely explanation is that the anisotropic properties of the reservoir overburden change over time.

Stress builds up in the Valhall overburden as a result of production-driven reservoir compaction. In turn, this stress is released by means of microseismic activity. Such a situation where stresses are built up continually and released in the Valhall overburden could explain the temporal changes in S-wave splitting. It also fits in well with our earlier conclusion that the seismic activity in cluster 1 is best explained in terms of multiple source mechanisms. Indeed, if the stresses change over time, then it is very conceivable that this could result in alternating motions on the same active fault area. Given the apparent random succession of events from different multiplet groups with time (Figure 5), it is likely that this cyclic charging and release of stresses occurs very rapidly.

Crampin (1994) postulates that large parts of the earth's crust are in a critical state, where small variations in stress and strain may lead to substantial changes in the behavior of the rock mass; such perturbations can be monitored easily by shear-wave splitting. Particularly in overpressured areas where pore pressures are close to confining pressures, it is likely that small stress changes temporarily close or pop open existing cracks, leading to temporal splitting variations. High-density fracture areas in cap rock are anticipated to exist close to large stress concentrations associated with fault zones. Clusters 1 and 2 are located on the intersection of two fault planes in Figure 10

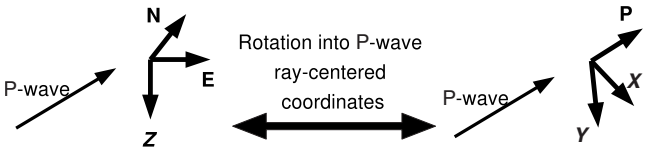

Figure 8. The 3-C data rotation into a P-wave ray-centered system. After rotation, the P-axis coincides with the P-wave ray direction. In Figure 7, the signal along this component is indicated in red. The *x*-axis is horizontal and perpendicular to the P-wave ray direction. The *y*-axis is perpendicular to both P and *x*. The *x*- and *y*-components of the multiplet stacked data in Figure 7 are green and blue. Nearly all recorded P-wave energy should be present on the P-component. If we ignore the effects of S-wave splitting and differences in raypaths between P- and S-waves, then most S-wave energy should be present on the *x*- and *y*-components. The S-wave energy partition between *x* and *y* will depend mainly on the source mechanism.

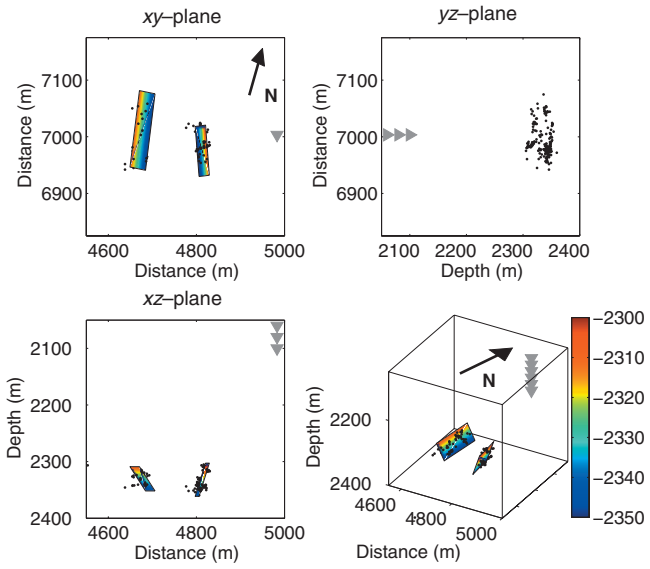

Figure 9. Relocated multiplet events from clusters 1 and 2 and previously shown in Figure 6b. A plane can be fitted to the source locations from each cluster. Both planes give the orientation and position of the possible fault planes on which the microseismic events occur. For both clusters, these inferred fault planes are subvertical and strike approximately north-northwest–south-southeast. More detailed fault parameters are provided in Table 2. The geophone locations are indicated by gray triangles.

Table 2. Best-fit planes to clusters 1 and 2. The reference coordinates give UTM coordinates and total vertical depth, referenced to mean sea level, of the clusters' centers of mass. They are also the midpoints of the fitted planes in Figure 9.

			Reference coordinates		
Cluster	Strike	Dip	*x*	*y*	*z*
1	−26°	68° W	4827	6926	2337
2	−11°	50° E	4695	6907	2333

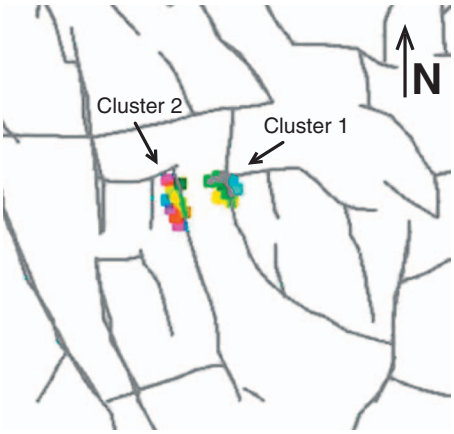

Figure 10. Events from clusters 1 and 2 on a top-reservoir fault map interpreted from 3D surface seismic data. The plot colors indicate the source depth rather than multiplet group. (Olav Barkved, personal communication, 2005)

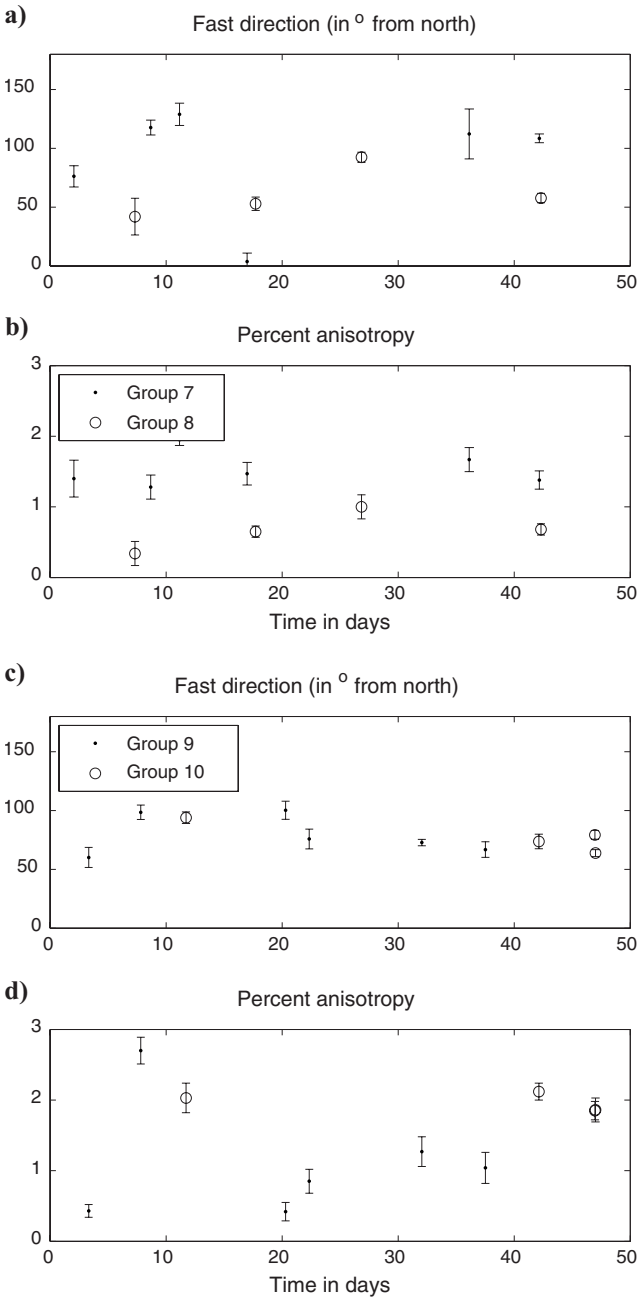

Figure 11. Comparison of S-wave splitting parameters from different multiplet groups. The fast S-wave polarization direction and percentage anisotropy for multiplet groups 7–10 are from Teanby et al. (2004). These groups all locate within cluster 1 on Figure 6, and their 3-C P-wave and S-wave stacks are provided in Figure 7. Groups 7 and 8 have on average (a) different fast directions and (b) percentage anisotropy values. Groups 9 and 10 have (c) similar fast directions but (d) different values of percentage anisotropy.

— precisely such an area of large stress concentration. The measured short-term variations in seismic anisotropy and the reactivation of microseismic source mechanisms over time of the individual events in these clusters thus point to a trigger mechanism of cyclic recharge and dissipation of cap-rock stresses in response to production-driven compaction of the underlying oil reservoir.

Additional evidence for this conjecture comes from the approximately 90° difference in fast polarizations for multiplet groups 7 and 8 (Figure 11). Such 90° flips are anticipated to occur given small variations in pore pressures or confining pressures if the effective pressure (i.e., confining pressure minus pore pressure) is close to 1–2 MPa (Crampin et al., 2002). In the Valhall cap rock, confining pressures are likely to change rapidly as a result of the production-driven compaction, e.g., by means of pore-space collapse within the reservoir, thereby inducing cyclic variations in cap-rock stresses and strains. Our findings emphasize the potentially large role of microseismic monitoring for constraining short-term variations in local stresses and strains within and around a reservoir.

CONCLUSIONS

Microseismic data contain abundant information on short-term variations in anisotropy, in situ stresses and strains, and earthquake locations and mechanisms. High-resolution absolute and relative event locations can be obtained by means of (1) crosscorrelation repicking of P-wave and S-wave arrival times and P-wave polarizations for each individual event, (2) identifying and removing P-wave polarization errors caused by rotating geophone tools, and (3) analyzing multiplets and crosscorrelating arrival-time repicking within each multiplet group.

This procedure reduces misfit and uncertainty estimates for event locations in the 1998 Valhall microseismicity by 50%, compared with a previous study, and reveals the existence of three additional source clusters; only the two largest clusters nearest the receiver were identified previously. Our analysis points to the existence of at least five seismically active fault zones within the overburden.

Events within the two main clusters lie approximately on a plane. The fault planes fitted through both clusters are subvertical and strike $-11°$ east and $-26°$ east. This is close to the known dominant fault-strike direction at Valhall. Inferred fault dips have a relatively large uncertainty but suggest a system of conjugate normal faults, which agrees well with the extensional stress state at Valhall.

Our multiplet analysis identifies 40 groups that comprise 208 of the 303 analyzed events. Several closely located multiplets show significant variations in their typical P-to-S amplitude ratios and S-wave phase content. This indicates the existence of different source mechanisms that reactivate over time. Strong correlations exist between some multiplet groups and the shear-wave splitting characteristics of the individual events comprising these groups (i.e., the time delay and fast polarization).

The integrated analysis of relocated sources, seismic multiplets, and S-wave splitting supports a model whereby stresses at Valhall recharge cyclically. Stress builds up in response to reservoir compaction as a result of oil production, and stress is released by means of microseismic activity. These changes cause variations in seismic anisotropy and the microseismic source mechanisms over time.

Our results thus illustrate the large potential of integrating S-wave splitting analysis with multiplet analysis and calculating accurate source locations in the context of monitoring reservoir stress. We anticipate that additional constraints on short-term variations of in situ stresses and strains can be obtained by analyzing microseismic source mechanisms. However, this will require more elaborate acquisition geometries where events are recorded at several wells, leading to a large range in source-receiver azimuth and incidence angles. Unfortunately, such an acquisition geometry was not available in the Valhall microseismic experiment.

ACKNOWLEDGMENTS

The authors would like to thank BP Norge, Shell Exploration and Production UK, and Schlumberger Cambridge Research for funding this research through the Leeds (now Bristol) Microseismicity Project. We are grateful to Olav Barkved from BP for providing material for Figure 10 and to Rob Jones for providing the initial suggestion for this work. We greatly appreciate helpful comments and suggestions from Steven Arcone, Alex van der Spek, Elmer Ruigrok, and Nancy House, and two anonymous reviewers.

REFERENCES

Al-Anboori, A., J.-M. Kendall, D. Raymer, and R. Jones, 2005, Microseismic monitoring and spatial variations in anisotropy, an example from Oman: 67th Conference and Technical Exhibition, EAGE, Extended Abstracts, P094.

Arrowsmith, S., and L. Eisner, 2005, A technique for identifying microseismic multiplets and application to the Valhall field, North Sea: Geophysics, **71**, no. 2, V31–V40.

Audigane, P., J.-J. Royer, and H. Kaieda, 2002, Permeability characterization of the Soultz and Ogachi large-scale reservoir using induced microseismicity: Geophysics, **67**, 204–211.

Bell, M., and H. Kaaijevanger, 2000, Integrated downhole monitoring of hydraulic fractured production wells: SPE European Petroleum Conference, 65156.

Crampin, S., 1994, The fracture criticality of crustal rocks: Geophysical Journal International, **118**, 428–438.

Crampin, S., T. Volti, S. Chastin, A. Gudmundsson, and R. Stefánsson, 2002, Indication of high pore-fluid pressures in a seismically active fault zone: Geophysical Journal International, **151**, F1–F5.

De Meersman K., M. van der Baan, and J.-M. Kendall, 2005, Automated signal extraction and polarization analysis on multi-component array data: Bulletin of the Seismological Society of America, **96**, 2415–2430.

Dyer, B., and R. Jones, 1998, 3D processing and interpretation of the microseismic data recorded during June and July 1998 in the Valhall field: CSM Associates Ltd. Internal Technical Report IR03/82.

Dyer, B., R. Jones, J. Cowles, O. Barkved, and P. G. Folstad, 1999, Microseismic survey of a North Sea reservoir: World Oil, **220**, 74–78.

Frémont, M., and G. Poupinet, 1987, Temporal variation of body-wave attenuation using earthquake doublets: Geophysical Journal of the Royal Astronomical Society, **90**, 503–520.

Gajewski, D., and E. Tessmer, 2005, Imaging of passive seismic sources by reverse modelling: 67th Conference and Technical Exhibition, EAGE, Extended Abstracts, C021.

Geller, R., and C. Mueller, 1980, Four similar earthquakes in central California: Geophysical Research Letters, **7**, 821–824.

Got, J.-L., 1994, Deep fault plane geometry inferred from multiplet relative relocation beneath the south flank of Kilauea: Journal of Geophysical Research, **99**, 15375–15386.

Hemmann, A., T. Meier, G. Jentzsch, and A. Ziegert, 2003, Similarity of waveforms and relative relocalisation of the earthquake swarm 1997/1998 near Werdau: Journal of Geodynamics, **35**, 191–208.

House, L., and R. Flores, 2002, Seismological studies of a fluid injection in sedimentary rocks, East Texas: Pure and Applied Geophysics, **159**, 317–401.

Jupe, A., R. Jones, S. Wilson, and J. Cowles, 2000, The role of microearthquake monitoring in hydrocarbon reservoir management: SPE Annual Technical Conference and Exhibition, 63131.

Kao, H., and S.-J. Shan, 2004, The source-scanning algorithm: Mapping the distribution of seismic sources in time and space: Geophysical Journal International, **157**, 589–594.

Kristiansen, T., O. Barkved, and P. Patillo, 2000, Use of passive seismic monitoring in well and casing design in the compacting and subsiding Valhall field, North Sea: SPE European Petroleum Conference, 65134.

Leonard, R., and J. Munns, 1987, Valhall, *in* A. M. Spencer et al., eds., Geology of the Norwegian oil and gas fields: Graham and Trotman, 154–163.

Lin, G., and P. Shearer, 2005, Tests of relative earthquake location techniques using synthetic data: Journal of Geophysical Research, **110**, B04304.

Maxwell, S., 1999, Relocation of Valhall microseismicity: BP-AmocoEngineering Seismology Group Internal Technical Report, AMOC002.

Maxwell, S., and T. Urbancic, 2002, Real-time 4D reservoir characterization using passive seismic data: SPE Annual Technical Conference and Exhibition, 77361.

Maxwell, S., R. Young, R. Busso, A. Jupe, and J. Dangerfield, 1998, Microseismic logging of the Ekofisk reservoir: SPE/ISRM International Conference, 47276.

Moriya, H., K. Nagano, and H. Niitsuma, 1994, Precise source location of AE doublets by spectral matrix analysis of triaxial hodogram: Geophysics, **59**, 36–45.

Moriya, H., H. Niitsuma, and R. Baria, 2003, Multiplet-clustering analysis reveals structural details within the seismic cloud at the Soultz geothermal field, France: Bulletin of the Seismological Society of America, **93**, 1601–1620.

Nolen-Hoeksema, R., and L. Ruff, 2001, Moment tensor inversion of microseisms from the B-sand propped hydrofracture, M-site, Colorado: Tectonophysics, **336**, 163–181.

Pavlis, G., 1992, Appraising relative earthquake location errors: Bulletin of the Seismological Society of America, **82**, 836–859.

Phillips, W., J. Rutledge, and L. House, 2002, Induced microearthquake patterns in hydrocarbon and geothermal reservoirs: Six case studies: Pure and Applied Geophysics, **159**, 345–369.

Poupinet, G., W. Ellsworth, and J. Frechet, 1984, Monitoring velocity variations in the crust using earthquake doublets: An application to the Calaveras fault, California: Journal of Geophysical Research, **89**, 5719–5731.

Ronen, J., and J. Claerbout, 1985, Surface-consistent residual static estimation by stack-power maximization: Geophysics, **50**, 2759–2767.

Rowe, C., R. Aster, W. Philips, R. Jones, B. Borchers, and M. Fehler, 2002, Using automated, high-precision repicking to improve delineation of microseismic structures at the Soultz geothermal reservoir: Pure and Applied Geophysics, **159**, 563–596.

Rutledge, J., W. Phillips, and M. Mayerhofer, 2004, Faulting induced by forced fluid injection and fluid flow forced by faulting: An interpretation of hydraulic-fracture microseismicity, Carthage Cotton Valley gas field, Texas: Bulletin of the Seismological Society of America, **94**, 1817–1830.

Scarfi, L., H. Langer, and S. Gresta, 2003, High-precision relative locations of two microearthquake clusters in southern Sicily, Italy: Bulletin of the Seismological Society of America, **93**, 1479–1497.

Schaff, D., G. Borkelmann, W. Elssworth, E. Zanzerkia, F. Waldhauser, and G. C. Beroza, 2004, Optimizing correlation techniques for improved earthquake location: Bulletin of the Seismological Society of America, **94**, 705–721.

Shapiro, S., E. Rothert, V. Rath, and J. Rindschwenter, 2002, Characterization of fluid transport properties of reservoirs using induced microseismicity: Geophysics, **67**, 212–220.

Teanby, N., J.-M. Kendall, R. Jones, and O. Barkved, 2004, Stress-induced temporal variations in seismic anisotropy observed in microseismic data: Geophysical Journal International, **156**, 459–466.

Waldhauser, F., and L. Elsworth, 2000, A double difference earthquake location algorithm: Method and application to the northern Hayward fault, California: Bulletin of the Seismological Society of America, **90**, 1353–1368.

Wolfe, C., 2002, On the mathematics of using difference operators to relocate earthquakes: Bulletin of the Seismological Society of America, **92**, 2879–2892.

Zoback, M., and J. Zinke, 2002, Production-induced normal faulting in the Valhall and Ekofisk oil fields: Pure and Applied Geophysics, **159**, 403–420.